Available online at www.sciencedirect.com
ScienceDirect
Fire Safety Journal 43 (2008) 442–450
FIRE SAFETY JOURNAL
www.elsevier.com/locate/firesaf

Flame size, heat release, and smoke points in materials flammability ☆

G.T. Linteris*, I.P. Rafferty

National Institute of Standards and Technology, Fire Science Division, 100 Bureau Dr., Stop 8665, Gaithersburg, MD 20899, USA

Received 25 July 2005; received in revised form 26 October 2007; accepted 28 November 2007
Available online 28 January 2008

Abstract

The concept of using the flame size as a surrogate for heat release rate (HRR) has been explored. A technique for simultaneously obtaining the HRR, flame size (height and area), and the smoke point of the flame solely from visual images has been developed. The technique has been demonstrated on gaseous flames (methane, propane, ethylene, and propylene) and explored for five burning solid polymers. Estimations of the flame *area* from images of the stoichiometric contour based on the CH chemiluminescent region of the flames yielded a good linear correlation with measured HRR, valid for all of the gaseous and solid compounds tested, for burning rates above or below the smoke point. In contrast, flame *heights* and luminous images (i.e., from soot emission) were confounded by differing behavior above and below the smoke point.
Published by Elsevier Ltd.

Keywords: Material flammability; Heat release rate; Flame size; Cone calorimeter

1. Introduction

The heat release rate (HRR) of a burning material is important for quantifying the growth and spread of a fire in a building [1], and effective methods for its measurement have been used extensively [2–4]. Nonetheless, if a faster screening method could be developed which allowed rapid, parallel, high-throughput testing, combinatorial methods might be applied to the problem of fire retardant development [5]. The height of co-flow laminar jet flames is known to be correlated with HRR [6–9], and work has recently appeared in which the reduction in flame size is used as a metric for fire retardant effectiveness [10]. Hence, it is useful to investigate the conditions under which flame size itself could be used as a more easily measured metric for heat release [11], as has been done for large fires [12]. Further, there is interest in using the method for situations for which HRR is desired, but capability for oxygen consumption calorimetry is not available (for example, in experiments to be flown aboard the International Space Station [13]). The purpose of the present work is to investigate the utility of flame size as a surrogate for HRR measurements on burning polymers, and to understand the limitations of the technique (since it is already being discussed by others for possible application).

2. Background

Flame size has been related to HRR indirectly in the past through work predicting the flame size as a function of fuel flow rate. Various researchers have analytically solved the conservation equations for mass, momentum, species, and energy with some approximations. The flames are modeled as 2-D, axisymmetric, laminar and steady, with infinitely fast chemistry, binary diffusion, and unity Lewis number, while neglecting buoyancy, radiation heat transfer, and axial transport (radial is included) [6–9,14]. Burke and Schumann [6] published the first analytical solution for the size of a jet diffusion flame. In their formulation the conservation equations for mass, species, momentum, and energy were essentially recast as a species conservation equation for a mixture fraction. Their assumptions included: no buoyancy, equal and constant velocity for the

☆ Official contribution of NIST, not subject to copyright in the United States.

*Corresponding author. Tel.: +1 301 975 2283; fax: +1 301 975 4052.
E-mail address: linteris@nist.gov (G.T. Linteris).

0379-7112/$ - see front matter Published by Elsevier Ltd.
doi:10.1016/j.firesaf.2007.11.006

fuel jet and co-flowing air, no radial velocity, infinitely fast kinetics, and constant gas density and diffusivity throughout the flame. Fay [7] extended the analysis to include variable density, and found that the predicted flame lengths were about 2.4 times those of the constant density solution. Roper [8] again extended the analysis assuming: constant temperature and diffusivity, unity Schmidt and Lewis numbers (i.e., equal rates for the diffusion of heat, mass, and momentum), and axial velocities which were constant for all radii. Chung and Law [14] included streamwise and preferential diffusion, and showed that these effects can be important for low Peclet number (*Pe*), i.e., low velocity, flows. Roper et al. [15] assembled experimental data from previous researchers and collected new data to verify their model. In their experiment, the height of the flame tip was determined from measurements of CO or soot disappearance, and they noted that the visible flame appearance is typically not a good marker for the stoichiometric flame contour.

Although the linear correlation between fuel addition rate and flame height is expected to hold for solid fuels, less work has been done to demonstrate this relationship, and there is reason to believe that the simplifying assumptions in the analytical descriptions could be less accurate for the flames over solid materials. For example, the analyses described above for flame size vs. fuel flow have typically concerned relatively high velocity, narrow, gaseous fuel jets, producing long, narrow flames (i.e., large aspect ratio). For solid material flammability, however, the flames will be wider and the fuel velocity at the surface will be lower. This increases the importance of axial diffusion (usually neglected in analytical descriptions). The lower fuel velocities reduce the Froude number, increasing the role of buoyancy, which has been shown to decrease flame widths due to radial convection (i.e., increased oxygen transport rates over molecular diffusion) [16]. Buoyancy-induced vortices also cause flame flicker, violating the assumption of a steady flame. Several properties of the burning materials will affect the assumption of infinitely fast gas-phase kinetics at the reaction sheet: (1) the materials will have a wide range of molecular structure, producing flames with varying sooting properties, and when added fire retardants are present, they too will produce incomplete combustion, and (2) heat losses to the fuel surface and from flame radiation (especially with sooting flames) will lower the flame temperature, again lowering the overall reaction rate. Hence, it is not clear a priori if all of the assumptions, which have been necessary for the analytical solutions for flame height as a function of fuel flow rate for gas jets will be justified for flames over condensed-phase materials. There have been no publications in which the measured HRR of a flame is compared with the flame size for burning condensed-phase materials, and the assumption of complete combustion of the fuel may need further consideration.

One useful measure of the completeness of combustion for fuels has been the laminar flame smoke point [17–20]. Measured in various ways, the smoke point is essentially the fuel flow rate for which the flame just begins to emit smoke, and it has been correlated with both the flame radiation heat losses and the incompleteness of combustion [21–23]. Hence, with regard to material flammability testing, the smoke point is a particularly important parameter, as has been described previously [24], since radiation heat losses, smoke formation, and combustion efficiency are all crucial parameters for fire modeling. The accuracy of the present correlations of flame size with HRR may depend upon the fuel generation rate with regard to the smoke point. Hence, it is necessary to consider the smoke point and if possible, measure it simultaneously.

The present work reports the flame height and flame area, together with the measured HRR for four gaseous and five polymeric fuels. The correlation between the flame size and the heat release is discussed, as is the smoke point and its relationship to the correlations developed. The utility of the present experimental technique for providing simultaneous measurement of the flame heat release and the smoke point for polymers is described.

3. Experiment

In order to produce flames which could be used in a combinatorial screening method, small laminar flames were employed. An experiment was designed for obtaining flame size and HRRs for steady flames of solid or gaseous fuels with measured mass consumption rates. The burner is shown schematically in Fig. 1. For gaseous fuels (Fig. 2), the burner is a variation of the cup burner [25,26], with a fuel "jet" consisting of a cylindrical glass cup (28 mm diameter) centered in a glass chimney (9.5 cm diameter). The fuel jet is made of pyrex (1.5 mm thick) and contains

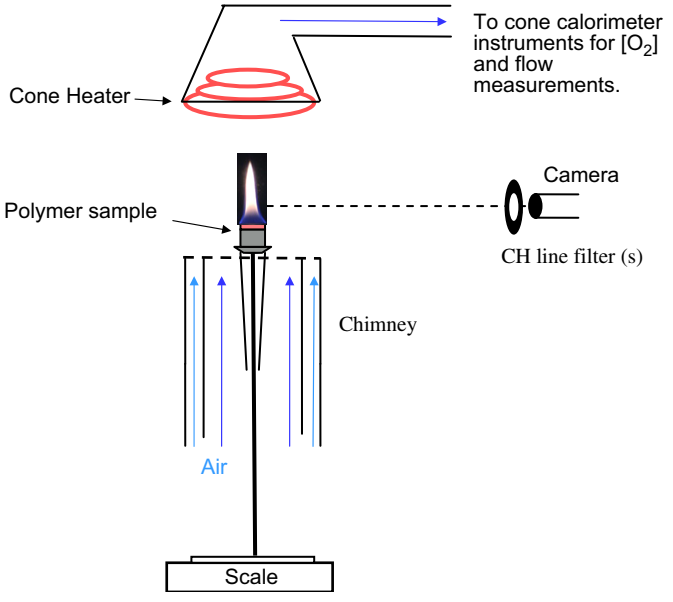

Fig. 1. Schematic of the laminar flow burner for testing polymer samples with radiant heating.

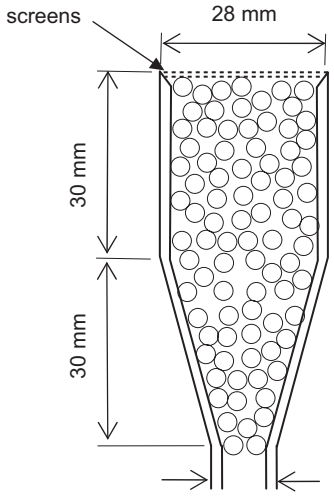

Fig. 2. Schematic diagram of the top of the burner used for gaseous fuels.

glass beads (3 mm diameter) with two screens (15.8 mesh/cm) on top to provide flow straightening. The co-flowing region contains a 10 cm thick bed of glass beads (6 mm diameter) to provide straightening for the oxidizer stream. For the polymer fuels, the burner is a variation of one used previously to study suppression of fires over solid materials [27]. The fuel is a solid sample (2.5 cm diameter and 2.5 cm tall), centered in an 8.5 cm dia. glass chimney; a scale (Mettler PE360[1]) measures the sample mass as a function of time. A radiant coil heats the solid samples to provide varying fuel supply rates. The heater is the same as that used in the cone calorimeter [4] but it is situated further from the sample (10–21 cm) so the flame image is not occluded by the cone heater. In both burners the chimney is cut off at a point just below the burner rim to avoid reflections during flame imaging. A co-flowing oxidizer stream (16.7 cm/s) helps to suppress flame flicker. Nonetheless, for the flame height measurements of the gaseous fuels, flame flicker was additionally suppressed using stabilizing screens [28]. There were six screens, 8 mesh/cm, 10 cm in diameter, with the first starting at the burner height, and each of the next located 2.54 cm above the previous. Each of the screens, in order, had a hole in the center of 40, 36, 32, 28, 24, and 20 cm diameter, with the largest hole in the lowest screen. For measurement of heat release, the exhaust products from either burner are directed to the hood of the NIST cone calorimeter, which uses oxygen consumption calorimetry [29]. To insure accurate results in the lower range of heat release characteristic of the cup burner, the exhaust fan speed of the cone was reduced by a factor of two from the ordinary setting (30 g/s), and the system was calibrated with controlled methane flows in the approximate heat release range of the reduced-scale samples (0.12–0.35 kW). For this heat release range, the measured HRR from the cone calorimeter is within 5% of that based on the heat release from the flame of a measured methane calibration flow (and within 10% at 0.05 kW). This agreement is considered good since the cone calorimeter itself, even at higher flows, has an uncertainty on the order of at least 5% [30]. Gas flows are measured by mass flow controllers (Sierra 860), which were calibrated so that their uncertainty is 2% of indicated flow. The fuels used were methane (Matheson UHP, 99.9%), propane (Matheson CP, 99%), ethylene, propylene (Matheson, CP), and various commercially available polymers, including acrylonitrile butadiene styrene (ABS), poly(methyl methacrylate) (PMMA), polypropylene (PP), high density polyethylene (HDPE), and polystyrene (PS). The air was house compressed air (filtered and dried), which is additionally cleaned by passing it through a 0.01 μm filter, a carbon filter, and a desiccant bed to remove small aerosols, organic vapors, and water vapor.

The flame size was determined with digital photography, using automated software to locate the flame contour and calculate the flame height or area. The flame images were recorded with a black and white charge coupled device CCD video camera (Sony, XC-ST50), coupled to a video frame-grabber board (with a resolution of 640×480 and a framing rate of 2 Hz) in a Pentium II-based personal computer. One or two interference filters, each with a bandpass of 10 nm centered at 430 nm (Oriel No. 59295) were used in series to isolate the emission line from excited CH radicals. This was done to facilitate imaging of the main reaction zone of the flame (which closely aligns with the stoichiometric contour) [31] rather than the luminosity from flame soot (which may not coincide with the stoichiometric contour). For comparison purposes, images were collected and analyzed with zero, one, or two filters. The flame images (obtained using two filters) were analyzed to determine the flame height, area, and volume using an automated image analysis system based on two software packages. The NASA image processing freeware program Spotlight 1.1 [32] provided the flame outline from the color image. A custom-written program subsequently interpreted the outline and calculated the flame surface area and volume. This process was repeated for each of the 30 frames of data and the results averaged.

For the small, non-flickering, nearly conical laminar flames, estimation of the flame height and area from the flame outline was straightforward, obtained by measuring the flame cord width at each height, and assuming axial symmetry, summing segments as described below. For convoluted flames typical of more turbulent conditions, the program was also capable of analyzing the flames using the method described by Orloff [33]. The total surface area or volume of the flame is the sum of all horizontal segments. Using this approach for complicated turbulent flame shapes, Orloff was able to produce flame areas within

[1]Certain commercial equipment, instruments, or materials are identified in this paper to adequately specify the procedure. Such identification does not imply recommendation or endorsement by NIST, nor does it imply that the materials or equipment are necessarily the best available for the intended use.

about 5% of those obtained from integration of the flame presence probability density function. Hence, we estimate that at the 95% confidence level, the luminous flame area for the small laminar flames (which have very regular shapes), have an uncertainty of less than 1%. Note that in many of the figures which follow, if the uncertainty is shown on the data points, the error bars represent the standard deviation (66% confidence level) for the variation in the flame area for the 30 frames of data (due to residual flame flicker). This uncertainty is much larger than that due to the flame area determination techniques described above.

For other measured parameters, an uncertainty analysis was performed, consisting of calculation of individual uncertainty components and root mean square summation of components. All uncertainties are reported as *expanded uncertainties*: $X \pm k u_c$, from a combined standard uncertainty (estimated standard deviation) u_c, and a coverage factor $k = 2$. Likewise, when reported, the relative uncertainty is $k u_c/X$. The expanded relative uncertainties for the theoretical heat release for the gaseous fuel flames (based on gas flow rates) are 4%. For the solid fuels, the heat release is measured by the cone calorimeter. Although the accuracy of that device is usually stated to be around 5%, at the low HRRs of the present measurements, our calibration runs with methane indicate that the combined relative uncertainty is about 10%.

4. Results and discussion

Using the reduced-scale laminar burner described above, flame images (with and without CH-line filters) at varying fuel flow (or generation) rates were collected for four gases and five polymers. The HRR using oxygen consumption calorimetery was obtained simultaneously, as was the fuel mass addition rate to the flame.

4.1. Gases

To understand and interpret the relationship between the measured visual flame size, heat release, and smoke point in the present laminar flames, we first conducted experiments using gaseous fuels. Experiments with methane, propane, ethylene, and propylene fuels provided a range of sooting tendency, and increasing fuel flow rates provided a range of flame size. For the soot-emitting flames (propane, ethylene, and propylene), the smoke point was determined (with stabilizing screens present) as the measured heat release at which the flame tip began to emit visible smoke. Visual images obtained using 0, 1, and 2 CH line filters in series with the CCD camera allowed discrimination between the region of soot particle blackbody emission (here called the luminous flame) and the main reaction zone of the flame (i.e., region of CH chemiluminescence), here referred to as the stoichiometric contour.

Results for four fuels are shown in the four plots in Fig. 3. In each plot for a given fuel, the flame area (open symbols) is given by the left scale, while the flame height (solid symbols) is given by the right scale; data for 0, 1, and 2 CH line filters are given by the circles, triangles, and squares. The uncertainty on the flame area or height grows with increasing HRR because the larger flames flicker more, yielding more frame-to-frame variation in the flame size (the stabilizing screens were used only for the manually determined smoke points). For methane, the smoke point HRR was beyond the range of the present tests (about 0.3 kW), whereas for propane, ethylene, and propylene, the smoke point HRRs were 0.31, 0.21, and 0.073 kW, and are indicated on the figures (dotted vertical line).

As all plots in Fig. 3 show, the inferred flame sizes with one or two filters are essentially the same. With 0 filters, however, the luminous flame image (from soot luminosity) is sometimes different from that with 1 or 2 filters, indicating that the soot-containing region does not always overlap with the stoichiometric contour of the flame. In the present work, the soot emission region is coincident with or larger than the image from the main reaction zone of the flame (i.e., the stoichiometric contour), in agreement with the results of Sunderland et al. [16], Mitchell et al. [34], and Gomez et al. [18], but in contrast to those of Roper et al. [15]. Further, the flame size determined from the luminous image compared to that from the stoichiometric contour depends upon the flame size relative to that at the smoke point. Below the smoke point, the flame sizes from the luminous flame and from the CH emission are essentially the same. For example, for methane (top left plot in Fig. 3), which is always below its smoke point in the present measurements (i.e., non-soot emitting) the flame height and area based on the luminous flame are slightly larger than the stoichiometric contour, but are quite close overall. For propane (top right in Fig. 3), the luminous and stoichiometric flame sizes are very close for all but the last few data points (which are near the smoke point). For the highly sooting flames of ethylene and propylene, however, behavior above and below the smoke point is clearly different. In both cases, below the smoke point flame size, the flame height or area with 0, 1, or 2 filters are essentially identical. Whereas above the smoke point fuel flow, the height and area are 23–47% larger when based on the luminous flame. These results are consistent with those of deRis and Cheng [24] for ethylene and propylene, which also show roughly linear variation of flame height with fuel flow rate below the smoke point (note that they use both a different burner configuration and smoke point determination method). Interestingly, both the present data as well as those of de Ris and Chang show that the flame height starts to change dramatically slightly below the fuel flow rate at which large amounts of soot are released. (Note also that the two experimental measurements, the smoke point determination and the flame size determination, are necessarily slightly different: the smoke point determination used stabilizing screens, but the flame size measurements could not (because the light scattered from the screens

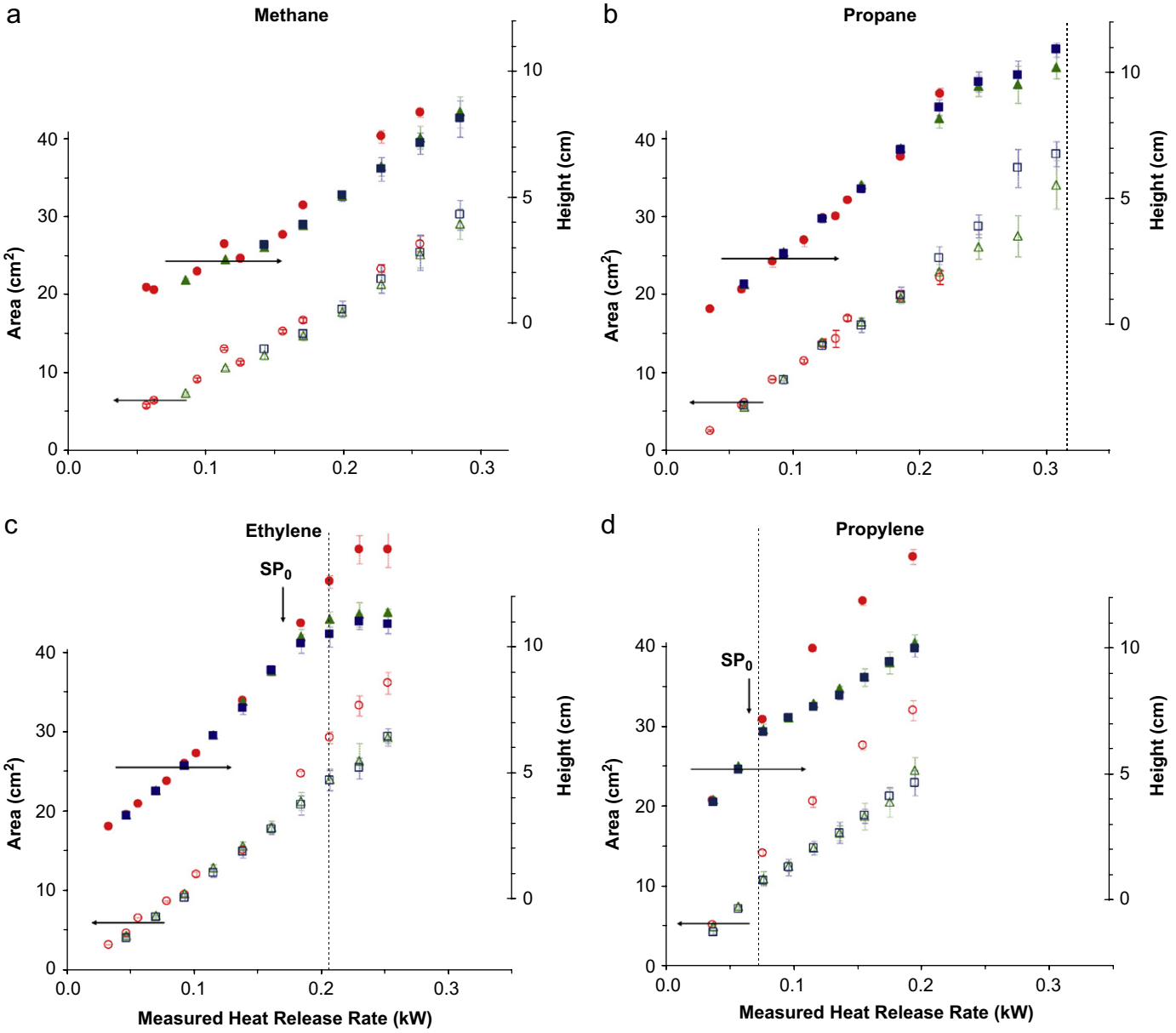

Fig. 3. Measured flame area (left scales) and height (right scales) with 0 (●), 1 (▲), or 2 (■) bandpass filters for (a) methane, (b) propane, (c) ethylene, and (d) propylene fuels. Dotted lines and small arrows marked SP_0 are the smoke point heat release rate, determined manually and with the optical imaging system.

interfered with the flame determination in the image processing). These differences may contribute to the discrepancy between the smoke points determined by the two techniques.)

The results in Fig. 3 indicate that use of *two* visual images (i.e., the luminous image and CH emission region) can determine the smoke point. Further, below the smoke point fuel flow rate, either flame *height* or flame *area* provides a linear relationship with the HRR, while above the smoke point, there is an apparent change in slope for the *height* versus the heat release, which is not as severe for the flame *area*. In general, flame area appears to be correlated with measured HRR better than does flame height.

As an example, the data in Fig. 3 from the present optical measurements can be used to determine the smoke point flame height (or HRR) for ethylene and propylene. In the lower two images of Fig. 3 for ethylene and propylene, the point at which the flame height determined with zero (closed red circles) or two (closed blue squares) filters diverges is marked with the arrow and labeled SP_0. These values for ethylene and propylene, 7.8 and 3.9 cm, are slightly lower than the smoke points determined based on manual, visual observations of the flame (with stabilizing screens) as described above.

For the four gaseous flames, the results of measurements of the stoichiometric flame size (height and area, using two filters) and the heat release are presented together in Fig. 4.

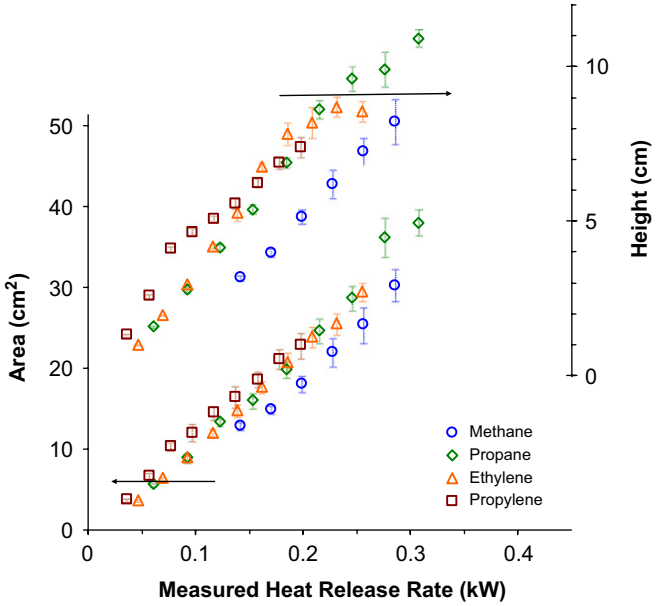

Fig. 4. Measured flame area (left scale) and height (right scale) with two filters vs. measured heat release rate for gases.

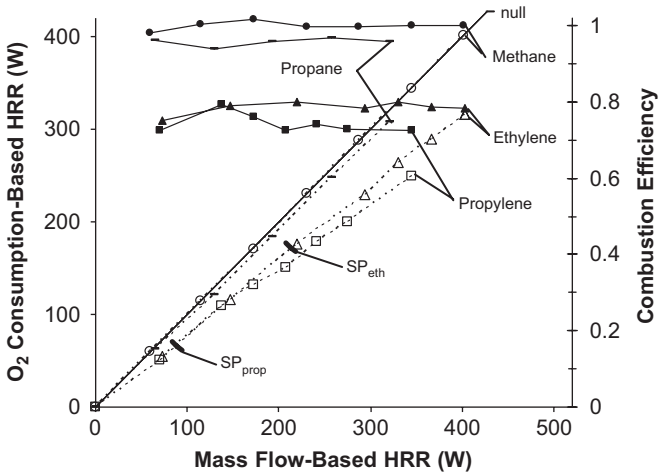

Fig. 5. Gaseous fuel heat release rate (HRR) from oxygen consumption calorimetry vs. that based on the fuel mass flow rate (open symbols, left scale) and the combustion efficiency (solid symbols, right scale).

Examining the upper assembly of data points (for flame height), the gaseous flames of propane, ethylene, and propylene all fall on the same linear curve, while those for methane (open circles) are noticeably smaller. For the flame area, the methane flames are again slightly smaller than the other gases, likely due to the higher mass diffusivity of methane compared to the other fuels, consistent with laminar flame theory [8]. Considering all of the gases together, the flame area is well correlated with the HRR ($r^2 = 0.95$), while the flame height is a little less well correlated ($r^2 = 0.85$).

The data used to generate Fig. 3 for the gaseous fuels can also provide data on the combustion efficiency as a function of flame size. For the four gaseous fuels, methane, propane, ethylene, and propylene, in the current laminar flame burner, the measured combustion efficiencies (based on the lower heating value) are shown in Fig. 5. These are calculated from the ratio of the measured HRR from oxygen consumption calorimetry and that based on the measured mass flow rate times the theoretical heat of combustion (lower heating value) of the fuel. For methane, the raw data of the HRR from O_2 consumption was about 4% higher than that based on the mass flow rate. In our data reduction, the combustion efficiency for methane was assumed to be unity, and that curve was used as a calibration curve for the system; that is, all values of HRR based on O_2 consumption for all fuels in Fig. 5 were lowered by 4%.

As Fig. 5 shows, the combustion efficiency for propane, ethylene, and propylene are about 0.96, 0.79, and 0.74, respectively. For these fuels, the combustion efficiency drops off for the lowest flow rate (perhaps due to increased heat loss and subsequent lower temperature in these smaller flames), while ethylene and propylene also show

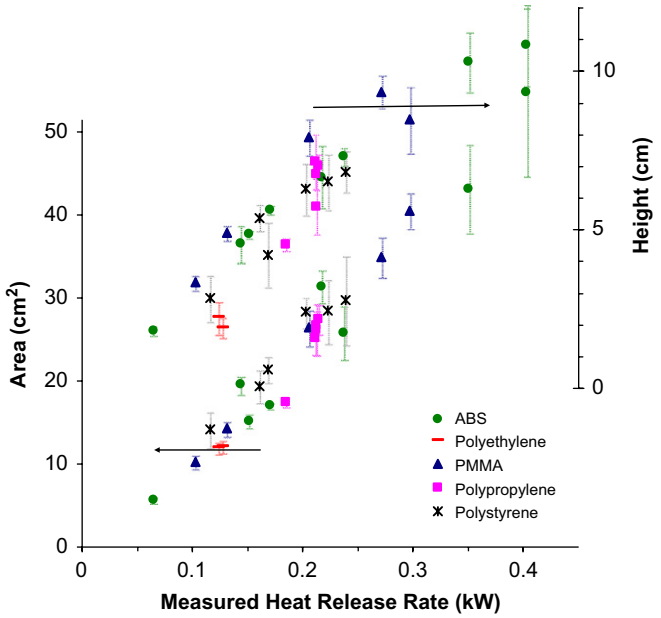

Fig. 6. Measured flame area (left scale) and height (right scale) with two filters vs. measured heat release rate for polymers.

decreases in the combustion efficiency as the flames grow significantly above their smoke point. These values of combustion efficiency compare to 0.95, 0.87, and 0.87, respectively, as reported by Tewarson [35] for flames in the FMRC Fire Propagation Apparatus (ASTM E2058: 10 cm × 10 cm burner size and turbulent conditions). Hence, the combustion efficiency in the present apparatus is lower than in the E2058 test (perhaps due to lower temperatures in the present apparatus from higher gas-phase conductive heat losses from the burning region). The lower measured combustion efficiency highlights the importance of both the heat losses from the flame, as well as the necessity of measuring the HRR from the flame rather than basing the heat release on the measured fuel consumption.

Table 1
Smoke point flame heights

Compound	Smoke point flame height (cm)				
	SFPE[a]	Present work		SFPE (converted[b])	Cheng and deRis[c]
		Manual visual	Automated optical		
Ethylene	9.7	12.0	7.8	10.2	13.7
Propylene	3.0	4.3	3.9	3.2	6.2
PMMA	10.5			11.0	6.8
PE	4.5			4.7	
PP	5.0			5.3	
PS	1.5			1.6	

[a]From Ref. [35].
[b]SFPE (converted) = SFPE × (7.8/9.7 + 3.9/3.0)/2.
[c]From Ref. [24].

4.2. Polymers

Data for the flame height and area (using two filters) as a function of the measured HRR for the polymers are also shown in Fig. 6. Data are presented for burning with an imposed heat flux from the radiant heater of 0 or 4.7 kW/m^2; the relatively low incident flux resulted from the need to position the cone heater relatively far above the sample (10–21 cm) so the flame was still visible. A varying net heat flux to the vaporizing polymer was obtained during the burn as the sample heated. As indicated, both the flame height and area are linearly related to the HRR, with the area ($r^2 = 0.96$) again better correlated than the height ($r^2 = 0.88$). Nonetheless, it is important to consider the smoke point of the burning polymers, since, as shown above and in Ref. [24], the flame shape relative to the HRR can change drastically above and below the smoke point.

Of the polymers tested here (PMMA, ABS, PE, PP, PS), there are data in the literature on the smoke point for all but ABS [35]. Table 1 shows the smoke point data from Ref. [35], together with that from Ref. [24] and the current results for ethylene and propylene from both the manual and automated optical techniques. As noted in Ref. [35], the values of smoke point are apparatus dependent. Hence, we have linearly scaled the values in Ref. [35] to our apparatus using the common results for ethylene and propylene, as shown in Table 1. The implied smoke point flame heights for PMMA, PE, PP, and PS are 11, 4.7, 5.3, and 1.6 cm, respectively. (Note that in our experiments, all of the ABS runs emitted visible smoke.) Comparing these values with the range of flame heights in the present tests (as shown in Fig. 4 for each compound), all data for PMMA and PE are below their smoke point, while the larger flow conditions for PP and all the data for PS and ABS are above their smoke point. Although sufficient data were not always available (described below) to determine the smoke point for the polymers using the optical method described above for ethylene and propylene, where data were available they were consistent with the smoke point flame heights just described. The important point is that the actual burning conditions of polymers will likely involve flame heights which are sometimes above and sometimes below the smoke points. Hence, it is important to have a flame size–HRR correlation method, which allows one to extract data for the whole range of fuel generation rates to be encountered in practice. As shown above for ethylene and propylene, the linear relationship for flame area (with two filters) vs. HRR is accurate both above and below the smoke point, while that for flame height is somewhat less accurate.

4.3. General considerations

An average value of the heat release per unit area of the flame can be extracted from the present results. From the data of Figs. 4 and 6 together, the inverse of the slope of the flame area versus the HRR gives a value of 80 kW/m^2. Based on an energy release per mass of O_2 or 13 100 kJ/kg [29], this value corresponds to mass flux of oxygen into the flames of 6.1 or 6.5 g/s/m^2, respectively. For our flames, the average value of the ratio of flame volume to flame area was 0.25 cm for propane, ethylene, and propylene, 0.32 cm for methane, and ranged from 0.25 to 0.45 cm for the polymers.

While the present work focused on the relationship between flame area and heat release, future work could help with several practical considerations related to the use of the technique as a screening method. These include: (1) unsteady and multi-dimensional heat losses in the sample, and (2) properties of the experimental flame imaging system. The unsteady heating of the polymer sample in the present tests was used as a means to obtain varying HRRs at a given incident radiant flux (that is, the time varying conductive losses to the thick sample changed the *net* heat input available for gasifying the sample). In actual practice, however, one typically wants to know the HRR at a given known *net* heat input. Hence, some means to insure a steady state condition (or estimate the conductive losses) would be necessary (for example, using thin samples of limited burning domain, as in Ref. [24]).

Similarly, 2-D heat losses from the edges of the sample will also change the net heat flux delivered from the radiant heating system. Some means would be necessary either to estimate these heat losses from the different samples or control them so they are the same for the different samples being screened. Finally, the imaging system in the present work could be improved by using a heater configuration, which does not occlude the flame at high fluxes. A more sensitive camera with a larger dynamic range would allow better resolution of the weak, blue regions of the flame simultaneously with the bright (even after filtering), sooting regions.

5. Conclusions

A method has been developed for simultaneously obtaining the flame size, heat release, and smoke point for flames over condensed-phase materials. From these, a correlation can be determined so that the HRR can be obtained solely from the optically measured flame area. Recorded images of the luminous flame (from soot emission) and that from CH emission (approximating the stoichiometric contour) diverge above the smoke point fuel addition rate so that the smoke point is readily determined. The flame area and the stoichiometric contour are found to be superior to the flame height and the luminous flame for correlating HRR. In addition, there exist several important considerations with regard to the actual implementation of the technique in a screening apparatus. For the small sample size here, account must be made of the unsteady and the multi-dimensional heat loss terms in the energy balance equation, since these can greatly reduce the effective heat input to the sample from the radiant source.

Acknowledgments

The authors thank Dr. Richard Lyon for his initial suggestion of using flame size as a measure of heat release rate for burning polymers. This research was supported by NIST and NASA's Office of Biological and Physical Research. One author (IPR) was supported by a NIST Summer Undergraduate Research Fellowship funded by the NSF.

References

[1] V. Babrauskas, R.D. Peacock, Heat release rate—the single most important variable in fire hazard, Fire Saf. J. 18 (1992) 255–272.
[2] A. Tewarson, Flammability of polymers and organic liquids, Part I, Burning intensity, Factory Mutual Research Corp., FMRC Serial 22429, Norwood, MA, 1975.
[3] B.A.L. Ostman, I.G. Svensson, J. Blomqvist, Comparison of 3 test methods for measuring rate of heat release, Fire Mater. 9 (1985) 176–184.
[4] W.H. Twilley, V. Babrauskas, User's guide for the cone calorimeter, National Institute of Standards and Technology SP-745, Gaithersburg, MD, 1988.
[5] J.W. Gilman, S. Bourbigot, J.R. Shields, M. Nyden, T. Kashiwagi, R.D. Davis, D.L. Vanderhart, W. Demory, C.A. Wilkie, A.B. Morgan, J. Harris, R.E. Lyon, High throughput methods for polymer nanocomposites research: extrusion, NMR characterization and flammability property screening, J. Mater. Sci. 38 (2003) 4451–4460.
[6] S.P. Burke, T.E.W. Schumann, Diffusion flames, Ind. Eng. Chem. 20 (1928) 998–1004.
[7] J.A. Fay, The distributions of concentration and temperature in a laminar jet diffusion flame, J. Aeronaut. Sci. 21 (1954) 681–689.
[8] F.G. Roper, Prediction of laminar jet diffusion flame sizes. 1. Theoretical model, Combust. Flame 29 (1977) 219–226.
[9] D.B. Spalding, Combustion and Mass Transfer. Pergamon Press, New York, 1979, pp., 185–195.
[10] J.M. Endtner, Development of new halogen-free flame retardant engineering plastics by application of automated optical investigation methods, in: 10th European Meeting on Fire Retardancy and Protection of Materials, Berlin, Germany, 2005.
[11] R. Lyon, FAA, Personal Communication, 2003.
[12] L. Orloff, J. de Ris, Froude modeling of pool fires, Proc. Combust. Inst. 19 (1982) 885–895.
[13] S. Olson, NASA, Personal Communication, 2003.
[14] S.H. Chung, C.K. Law, Burke–Schumann flame with streamwise and preferential diffusion, Combust. Sci. Technol. 37 (1984) 21–46.
[15] F.G. Roper, C. Smith, A.C. Cunningham, Prediction of laminar jet diffusion flame sizes. 2. Experimental verification, Combust. Flame 29 (1977) 227–234.
[16] P.B. Sunderland, B.J. Mendelson, Z.G. Yuan, D.L. Urban, Shapes of buoyant and nonbuoyant laminar jet diffusion flames, Combust. Flame 116 (1999) 376–386.
[17] R.L. Schalla, R.R. Hubbard, Smoke and coke formation in the combustion of hydrocarbon–air mixtures, NASA NACA Report 1300, 1959.
[18] A. Gomez, G. Sidebotham, I. Glassman, Sooting behavior in temperature-controlled laminar diffusion flames, Combust. Flame 58 (1984) 45–57.
[19] J.H. Kent, A quantitative relationship between soot yield and smoke point measurements, Combust. Flame 63 (1986) 349–358.
[20] M.A. Delichatsios, Smoke yields from turbulent buoyant jet flames, Fire Saf. J. 20 (1993) 299–311.
[21] G.H. Markstein, Relationship between smoke point and radiant emission from buoyant turbulent and laminar diffusion flames, Proc. Combust. Inst. 20 (1985) 1055–1061.
[22] A. Tewarson, Smoke-point flame height and fire properties of materials, Factory Mutual Research Corp., FMRC Technical Report J.I. OK3R3.RC, NIST-GCR-88-555, Norwood, MA, 1988.
[23] L. Orloff, J. de Ris, M.A. Delichatsios, Radiation from buoyant turbulent-diffusion flames, Combust. Sci. Technol. 84 (1992) 177–186.
[24] J. de Ris, X.F. Cheng, Role of smoke-point in material flammability testing, International Association for Fire Safety Science, in: Proceedings of the 4th International Symposium, Ottawa, Ontario, p. 301.
[25] B. Hirst, K. Booth, Measurement of flame extinguishing concentrations, Fire Technol. 13 (1977) 296–315.
[26] G.T. Linteris, G.W. Gmurczyk, Prediction of HF formation during suppression, in: R.G. Gann (Ed.), Fire Suppression System Performance of Alternative Agents in Aircraft Engine and Dry Bay Laboratory Simulations, National Institute of Standards and Technology, Gaithersburg, MD, 1995, pp. 201–318.
[27] M.K. Donnelly, W.L. Grosshandler, Suppression of fires exposed to an external radiant flux, National Institute of Standards and Technology, NIST IR 6827, Gaithersburg, MD, 2001.
[28] J.H. Kent, H.G.G. Wagner, Why do diffusion flames emit smoke?, Combust. Sci. Technol. 41 (1984) 245–269.
[29] C. Huggett, Estimation of rate of heat release by means of oxygen-consumption measurements, Fire Mater. 4 (1980) 61–65.
[30] V. Babrauskas, Development of the cone calorimeter—a bench-scale heat release rate apparatus based on oxygen-consumption, National Bureau of Standards, NBSIR 82-2611, Gaithersburg, MD, 1982.

[31] K.T. Walsh, M.B. Long, M.A. Tanoff, M.D. Smooke, Experimental and computational study of CH, CH*, and OH* in an axisymmetric laminar diffusion flame, Proc. Combust. Inst. 27 (1998) 615–623.

[32] R. Klimek, T. Wright, Spotlight 1.1, NASA Glenn Research Center, Cleveland, OH, 2002.

[33] L. Orloff, Simplified radiation modeling of pool fires, Proc. Combust. Inst. 18 (1981) 549–583.

[34] R.E. Mitchell, A.F. Sarofim, L.A. Clomburg, Experimental and numerical investigation of confined laminar diffusion flames, Combust. Flame 37 (1980) 227–244.

[35] A. Tewarson, Generation of heat and chemical compounds in fires, in: C.L. Beyler, R.L.P. Custer, W.D. Walton, J.M. Watts Jr., D. Drysdale, J.R. Hall Jr., P.J. Dinenno (Eds.), SFPE Handbook of Fire Protection Engineering, National Fire Protection Association, Quincy, MA, 1995, 3-53–3-124.